UC Berkeley

Microgravity Combustion

Title

Laser Extinction in Laminar Inverse Diffusion Flames

Permalink

https://escholarship.org/uc/item/5xq8441t

Authors

Macko, Kevin
Mikofski, Mark A
Fernandez-Pello, Carlos
et al.

Publication Date

2005-10-18

Peer reviewed

Laser Extinction in Laminar Inverse Diffusion Flames

Kevin T. Macko*, Mark A. Mikofski, A. Carlos Fernandez-Pello
University of California, Berkeley

Linda G. Blevins[†]
Sandia National Laboratories, Livermore, CA

Ronald W. Davis
National Institute of Standards and Technology (retired), Gaithersburg, MD

*Corresponding Author: macko@berkeley.edu

[†]Current Address: National Science Foundation, Arlington, VA

Laser Extinction in Laminar Inverse Diffusion Flames

Kevin T. Macko, Mark A. Mikofski, A. Carlos Fernandez-Pello
University of California, Berkeley

Linda G. Blevins
Sandia National Laboratories, Livermore, CA

Ronald W. Davis
National Institute of Standards and Technology (retired), Gaithersburg, MD

Abstract
Measurements of line-of-sight laser extinction in a co-annular ethylene-air laminar inverse diffusion flame (IDF) were made to determine soot concentration. Extinction has frequently been used in the literature to measure soot concentration in normal diffusion flames (NDFs), but it has rarely been applied to IDFs. A coflow IDF contains a primary air flow surrounded by a fuel annulus. Soot particles form on the outside of IDFs, advect upward, and eventually quench without being oxidized. It has been proposed in the literature that IDFs will produce less near-flame soot than NDFs because, for flames of comparable fuel, size and flow rates, movement of soot outward into cool regions of an IDF limits its simultaneous exposure to the high temperatures and fuel pyrolysis products needed for soot growth. A two-dimensional soot concentration map of an IDF using experimental data confirms this hypothesis by showing integrated soot volume fractions to be an order of magnitude lower than those reported for NDFs in the literature. Computer simulations of particle temperature histories in an NDF and IDF of similar height lend support to these results.

Introduction

Inverse diffusion flames (IDFs) are similar to normal diffusion flames (NDFs), with the main difference being that the locations of fuel and oxidizer are reversed. Instead of fuel being injected into an excess of air, a jet of air is sent into an excess of fuel. This configuration allows the combustion process to resemble conditions seen in underventilated fires, in which combustion is fuel rich and large amounts of CO, soot and other carbon containing species are produced and not oxidized. IDFs and underventilated NDFs are expected to have similar soot pathways. Most notably, in both cases the soot never passes through a closed flame tip [1]. With the IDF configuration, since soot forms on the fuel side of the flame, most of the soot particles do not pass through this high temperature zone, escaping unoxidized [2]. IDFs thus provide the opportunity to study soot precursors and incipient soot since the soot formation process is halted before oxidation would occur in an NDF.

The study of soot particles and their formation process is important for a number of reasons. Soot emitted from internal combustion engines and industrial combustors have led to health concerns related to inhalation of particulate matter [3]. Accidental fires are also affected by soot, in that their propagation often involves radiant heat transfer from hot soot particles [4]. Therefore, a better understanding of the soot that exists in underventilated combustion may lead to future improvements in particulate emissions and fire safety.

The aim of this study is to investigate soot concentration in an IDF from a cylindrical co-flowing burner with line-of-sight laser extinction measurements. An advantage of this extinction technique is that small concentrations of soot can be measured readily, due to the relatively large optical cross sections of soot particles, which facilitate light extinction [5]. This is especially important for IDFs, where it has been reported that soot concentrations in the flame are an order of magnitude lower than those in NDFs (~1 ppm in IDFs [6] and ~8-18 ppm in NDFs [7,8]). The experimental apparatus is also straightforward in its setup and costs relatively little to implement. Laser extinction has been used extensively in the investigation of NDFs to yield soot volume fraction data directly [7,9]. It has also been used to calibrate full-field soot Laser-Induced Incandescence (LII) measurements in NDFs for soot volume fraction [8,10], which has the advantage of providing time-resolved and spatially-resolved data. Shaddix *et al.* [2] measured soot concentrations using LII calibrated with laser extinction in a slot IDF and examined the sooting characteristics of steady and pulsed IDFs. Limited soot laser extinction measurements have been attempted with cylindrical co-flowing IDFs. Makel and Kennedy [6] applied laser extinction on an enclosed cylindrical IDF burner with relatively high velocity air flow, which required the use of a stabilizing hydrogen pilot flame. To the authors' knowledge, this past study is the only one that reports laser extinction measurements in a coflow IDF.

The objective of this paper is to gain more insight into IDFs with the laser extinction method using a different IDF burner and fuel and air flow rates different from those used by Makel and Kennedy and Shaddix *et al.* The burner design eliminates potential edge effects that can occur with enclosed burners. A computational model is employed to

predict mixture fractions, temperatures, and soot time-temperature histories for comparison with the measured soot concentrations.

Experimental Apparatus & Methodology

The co-annular IDF jet burner used in this study has been described in detail by Blevins *et al.* [1] and can be seen in Fig. 1. The burner consists of a central 1.0-cm diameter air tube surrounded by an annular 3.0-cm diameter fuel tube. To prevent an outer diffusion flame between the fuel and the surrounding air, a 6.4-cm diameter jet of nitrogen flowed around the outside of the fuel jet. Over a typical flame height of 2 cm, momentum from the nitrogen would be transferred approximately one millimeter into the fuel stream [11].
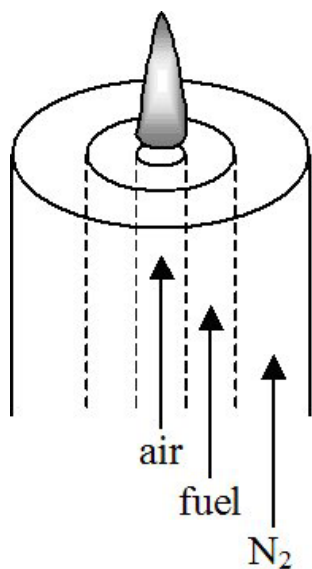

Figure 1. Schematic of IDF Burner

Thus, the effect of nitrogen on the flame was considered negligible. All flow rates were held constant during the experiment. The rates of flow were 2.2 slpm of air, 2.7 slpm of ethylene, and 30 slpm of nitrogen, where slpm refers to standard liters per minute at a standard condition of 101 kPa and 293 K. The average cold-flow velocities were estimated to be 47 cm/s, 7.2 cm/s, and 20 cm/s respectively. These flow rates were chosen for their observed flame stability and relatively high propensity to soot as observed by Mikofski *et al.* [11]. The air and fuel flow rates were controlled by mass flow controllers (Sierra Instruments model 810C), and the nitrogen was controlled by a rotameter (Omega model FL-3840). Since a significant amount of unburned fuel was released by the IDF burner, a methane flare was used far downstream of the burner in the hood exhaust to prevent the unburned fuel from passing into the laboratory exhaust duct. To avoid recirculation zones that could possibly affect the flame, no surrounding shields were used directly next to the IDF. However, to prevent crosscurrents from making the flame unstable, vinyl film curtains were placed about two feet from the burner around the experiment, and care was taken to ensure that disturbances in the room were kept to a minimum.

The optical arrangement for the laser extinction measurements is shown in Fig. 2. The light source was a 10 mW helium-neon laser (Uniphase model 1135) operating at a wavelength of $\lambda = 632.8$ nm. A mechanical chopper (Stanford Research Systems model SR540) modulated the laser beam at a frequency of 500 Hz. The laser beam was chopped so that a lock-in amplifier could detect and amplify the 500 Hz signal, thus increasing the signal-to-noise ratio. To facilitate alignment of the laser beam, two adjustment mirrors were used. The laser beam then passed through a 17-cm focal length focusing lens prior to traversing through the IDF. The laser beam diameter was approximately 0.5 mm across the sampling volume of the flame. Past the IDF was

another focusing lens, a neutral density filter, a laser line interference filter centered at the operating wavelength, an iris aperture, and a silicon photodetector (Edmund Optics model NT53-373). The optical instruments used to collect the laser beam after it passed through the IDF were surrounded by a reflective aluminum box to prevent ambient light and radiant heat sources from interfering with the photodiode measurements. The signal from the photodiode and the chopper frequency were sent to a lock-in amplifier (Stanford Research Systems model SR530) operating with a 1-ms time constant. The lock-in amplifier processed the signal and sent it to a computer for data acquisition.
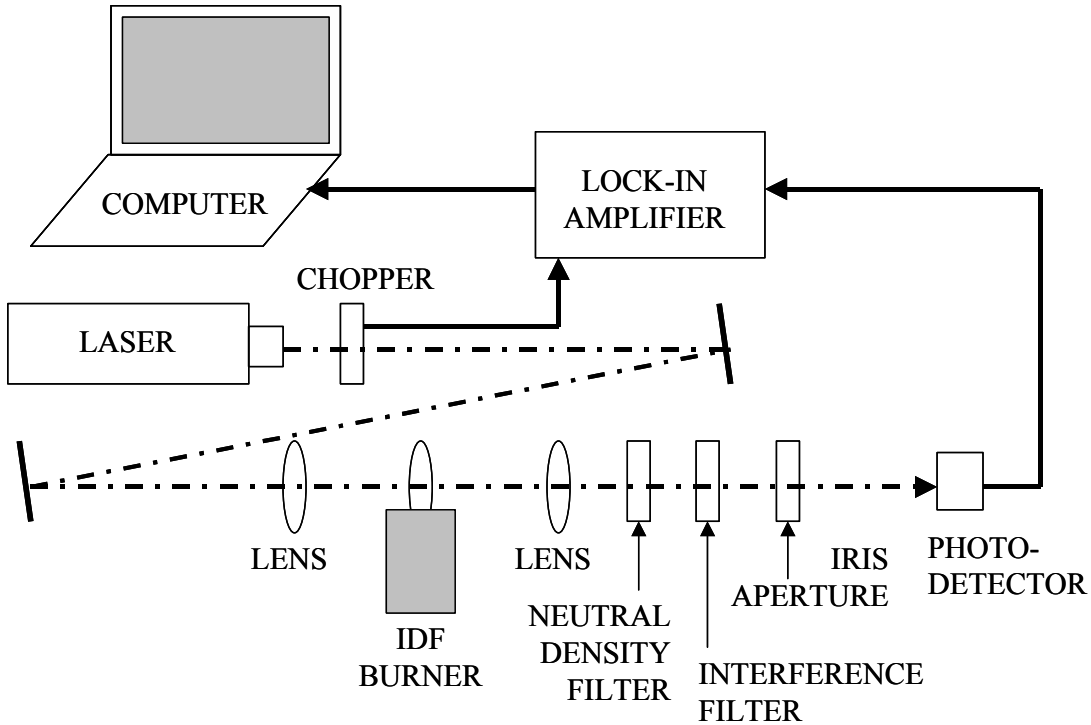

Figure 2. Experimental Setup

During experiments, all of the optics were stationary on an optical table, and the IDF burner was moved horizontally at 0.25 mm spacing using a single-axis translation stage with a precision of 0.01 mm. The burner was traversed so that measurements could be made across the entire width of the flame. Photodiode output was recorded for three seconds at a sampling frequency of 1000 Hz while the IDF was on, and then the data were averaged. After the flame was extinguished, one second of photodiode data was recorded and averaged to determine the baseline incident laser intensity. This process was performed three times at each horizontal location to provide an average value. Heights above the burner of 15, 20, 25, and 30 mm were examined by adjusting the burner on a vertical positioning lift with a measurement precision of 0.5 mm. The height of the flame is about 22 mm, based on simulations described later in this paper. Normalizing by the flame height, the measurement locations of 15, 20, 25, and 30 mm correspond to 0.7, 0.9, 1.1, and 1.3 times the flame height, respectively.

4

Following the acquisition of projection data, high frequency spatial fluctuations were filtered out of the data using a third order low-pass digital Butterworth filter that removed frequencies greater than 1/8 the spatial sampling frequency (four data points per millimeter). In addition, both sides of the flame were averaged across the centerline. The filtering and averaging were necessary to provide a relatively smooth curve for deconvolution, which is extremely sensitive to noisy data. The deconvolution algorithm converted the line-of-sight path integrated data into a spatial field of extinction coefficients. An onion-peeling tomographic inversion [12] was performed for each sampled height above the burner. The extinction coefficient at each radial position was determined by using Bouguer's Law:

$$\frac{I}{I_0} = e^{-k_{ext}l}$$

Eq. 1

where I (V) is the incident laser intensity measured by the photodetector with the flame on, I_0 (V) is the laser intensity with the flame off, k_{ext} (1/mm) is the local laser extinction coefficient, and l (mm) is the pathlength of the laser through the sampling volume. Soot volume fractions, f_v, could then be calculated using the following equation [13]:

$$f_v(r) = \frac{k_{ext}(r)\lambda}{6\pi E(\widetilde{m})}$$

Eq. 2

where λ (mm) is the laser wavelength, and $E(\widetilde{m})$ is a function of the refractive index of the soot. The use of this equation assumes that the soot particles are within the Rayleigh size limit, and hence the scattering contribution to the total measured extinction is negligible. For this study, an index of refraction of $\widetilde{m} = 1.57 - 0.56i$ was used as suggested by Smyth and Shaddix [14]. The true value of soot's refractive index has been debated in the literature, and it has been reported to be slightly affected by such conditions as temperature [15,16], C/H ratio, and extent of agglomeration [14]. Blevins *et al*. [1] observed that post-flame IDF soot has a lower C/H ratio than typical NDF post-flame soot. Therefore, IDF soot is likely to have a different index of refraction than NDF soot, but our current understanding of this remains limited. Thus, for ease of comparing results to previous studies, the common value of $\widetilde{m} = 1.57 - 0.56i$ for soot refractive index was used. This uncertainty in the refractive index propagates into uncertainty of the calculated soot volume fractions.

Computational Methods
To put the laser extinction results into context in the IDF, a computer simulation was run to model temperature and mixture fraction profiles. With this information, the location of measured soot concentrations could be compared to the contour locations of minimum soot formation temperature (reported in the literature as approximately 1300 K [17-19]) and stoichiometric mixture fraction (0.0638 for ethylene-air). Calculations were carried out using direct numerical simulation of the time-dependent Navier Stokes and conserved variable equations for an axisymmetric laminar flame [20]. The simulation employed

assumptions of low Mach number, infinite-rate chemical kinetics, unity Lewis number, variable thermophysical properties, a semi-infinite surrounding fuel-stream, and negligible radiation heat transfer. Predicted flame heights from the simulation agreed within 10% of previously measured flame heights [11]. The simulation was also tested by comparing predicted and measured axial temperatures [21]. The model underpredicted temperatures at the centerline near the base of the flame, and overpredicted the peak temperature, but agreed well with measurements everywhere else. While the model assumes fuel and air exit the burner at ambient temperature, heat transfer at the base of the flame causes slight preheating of the reactants. The model overpredicts the peak temperature because it neglects heat losses due to radiation and also assumes that the only products of combustion are CO_2, H_2O, and N_2. Considering only these products and performing chemical equilibrium calculations (STANJAN) yields an adiabatic flame temperature for a stoichiometric ethylene-air mixture of 2566 K, which agrees well with the maximum temperature obtained in the simulation. This temperature is higher than the adiabatic flame temperature for ethylene of 2369 K computed assuming dissociation of the combustion products.

The model includes dilute-condition particle tracking, incorporating the effects of inertial, thermophoretic, and gravitational forces [22]. Tracer particles, 40 nm in diameter and with the properties of amorphous carbon [23], were introduced at an axial position of 3 mm above the burner, corresponding to the base of the visible soot cone in the ethylene-air IDF, and at radial positions corresponding to gas temperatures of 1300 K and 1900 K. These temperatures were chosen based on the lower temperature limit for soot formation of 1300 K reported in the literature [17-19], and a proposed hypothetical upper limit for soot formation of 1900 K based on the measurements of laser extinction presented in the results section of this paper. The analysis of the computational results assumes that soot mass increases, either through inception or surface growth, between these two limiting temperatures of 1300 K and 1900 K. Although the simulation does not model soot formation, the trajectories and time temperature histories of the tracer particles were used to mimic soot particles passing through the flame. Therefore, the tracer particles in the NDF were tracked until they reached the stoichiometric contour (mixture fraction of 0.0638), where the soot particles would be oxidized. However, for the IDF the particles continued until they exited the computational domain (height of 5 cm) because they are always in the fuel stream and never cross the reaction zone to react with oxygen. Although the predicted trajectories and time-temperature histories of the tracer participles are qualitative, they serve as a theoretical tool for discussing the differences in soot residence time at high temperature and its effect on soot formation in NDF and IDFs.

Results and Discussion

The raw projection laser extinction data are shown in Fig. 3, along with vertical bars showing the standard deviation in the average of three measurements at each location. The minimum transmittance (I/I_0) in the IDF was approximately 97%, which is indicative of low soot concentrations when compared to reported values of about 70% transmittance for ethylene NDFs [7]. These low levels of extinction lowered the signal-to-noise ratio and led to data with relatively large standard deviations. Some of the

variability in the data is attributed to slight instabilities in the IDF, with some small flickering and wobble observed. However, a clear trend can still be seen, with two soot peaks at the outer edges of the flame, and the soot levels approaching zero farther out into the fuel stream.
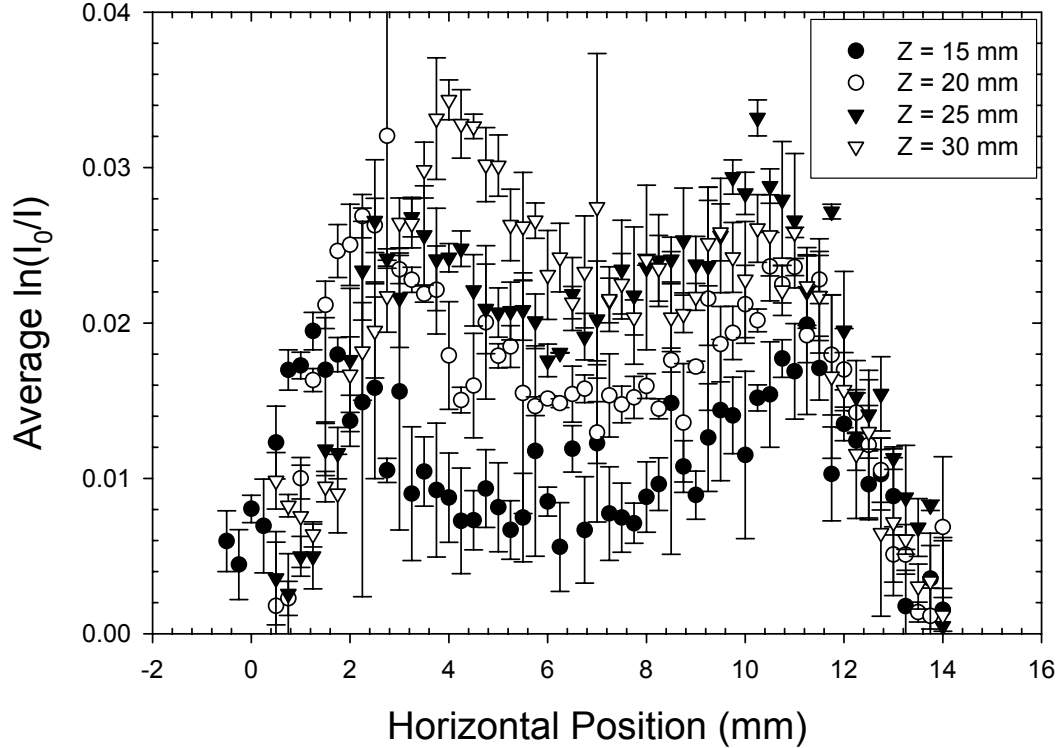

Figure 3. Raw Projection Data with Vertical Uncertainty Bars

Figure 4 shows the radial profile of the measured soot volume fraction along with the simulated mixture fraction profile for the height of 15 mm (0.7 of flame height) above the flame. The estimated maximum uncertainty for soot volume fraction, calculated by combining the photodetector uncertainty, estimated extinction pathlength and deconvolution uncertainty, soot index of refraction uncertainty, and the standard deviation of the unattenuated laser beam intensity, is 0.08 ppm and is represented in the plot by the vertical bar at the soot peak. Dotted horizontal and vertical lines show value and location of the ethylene-air stoichiometric mixture fraction (0.0638). As expected, the soot concentration is zero on the air side of the stoichiometric mixture fraction/maximum temperature contour of the flame. As radial distance increases, soot volume fraction increases to a peak value of 0.27 ppm at a radius of 5.2 mm and then decreases. Mixture fraction increases uniformly with increasing radius. The computed mixture fraction at the location of the peak soot volume fraction is 0.26.
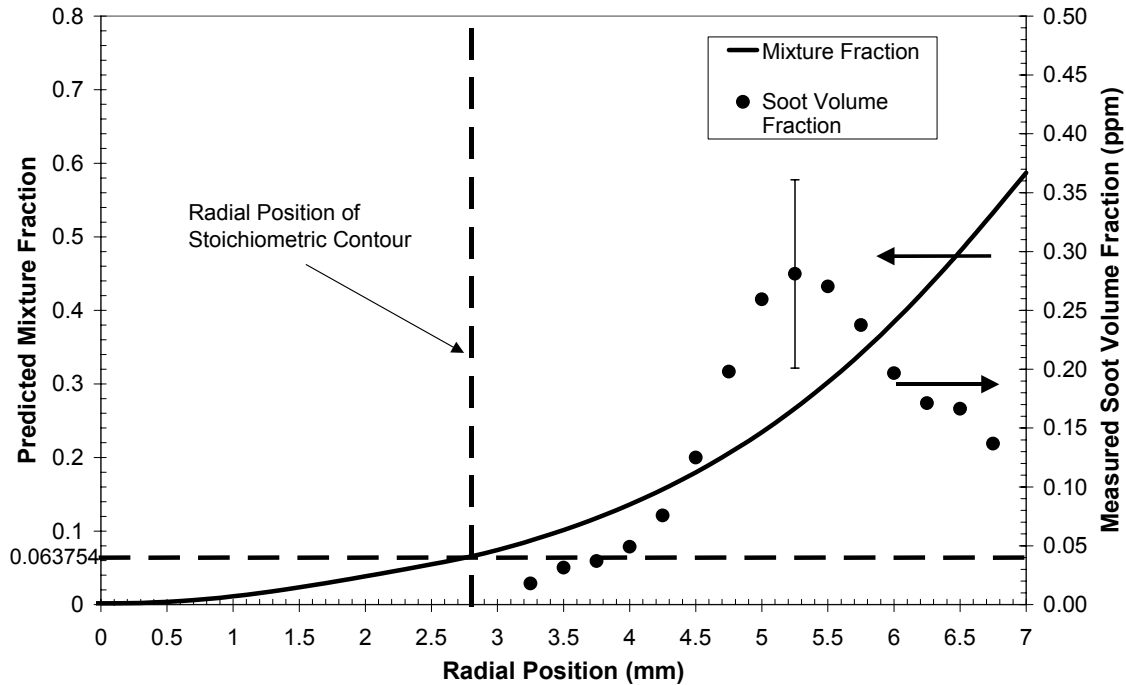
Figure 4. Measured Soot Volume Fraction and Predicted Mixture Fraction at 15-mm Axial Position, Ethylene IDF, 2.2-slpm Air

Figures 5-7 show measured soot volume fractions and predicted mixture fractions for vertical distances of 20 mm (0.9 of flame height), 25 mm (1.1 of flame height), and 30 mm (1.3 of flame height). The trends of soot volume fraction and mixture fraction are similar to those in Fig. 4. Lines marking the stoichiometric mixture fraction are absent from Figs. 6-7 because these measurements are taken above the flame tip. The soot volume fraction plots in Figs. 5-7 have small peaks near the centerline and away from the main soot peak. This is a non-physical effect and is attributed to noise from the extinction data that have passed through the deconvolution process; the onion-peeling deconvolution technique becomes increasingly sensitive to noise in the input data as the radius approaches zero. For the height of 20 mm in Fig. 5, soot volume fraction peaks at a value of 0.40 ppm at a radius of 5.0 mm, corresponding to a mixture fraction of 0.25. For the height of 25 mm in Fig. 6, soot volume fraction peaks at a value of 0.40 ppm at a radius of 4.5 mm, corresponding to a mixture fraction of 0.22. For the height of 30 mm in Fig. 7, soot volume fraction peaks at a value of 0.44 ppm at a radius of 3.8 mm, corresponding to a mixture fraction of 0.23. The radial locations of the soot concentration peaks decrease with axial height because soot particles follow the streamlines inward toward the centerline as they move downstream in the flame and past the flame tip. In summary, peak soot volume fractions have values between 0.25 and 0.45 ppm, occurring when the mixture fraction is between 0.22 and 0.26 (rich of stoichiometric). The peak soot concentrations on the order of one part per million have values consistent with the order of magnitude of those measured for IDFs previously [2,6] and considerably lower than the peak soot concentrations reported for coflow NDFs of 8-18 ppm [7,8].
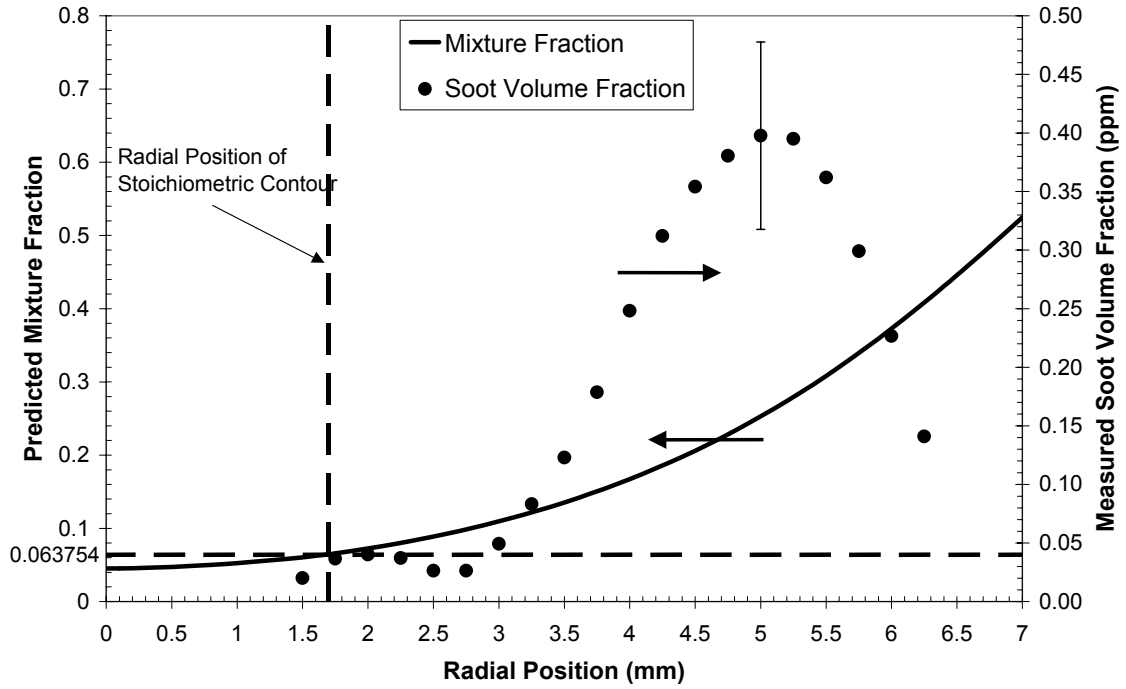
Figure 5. Measured Soot Volume Fraction and Predicted Mixture Fraction at 20-mm Axial Position, Ethylene IDF, 2.2-slpm Air
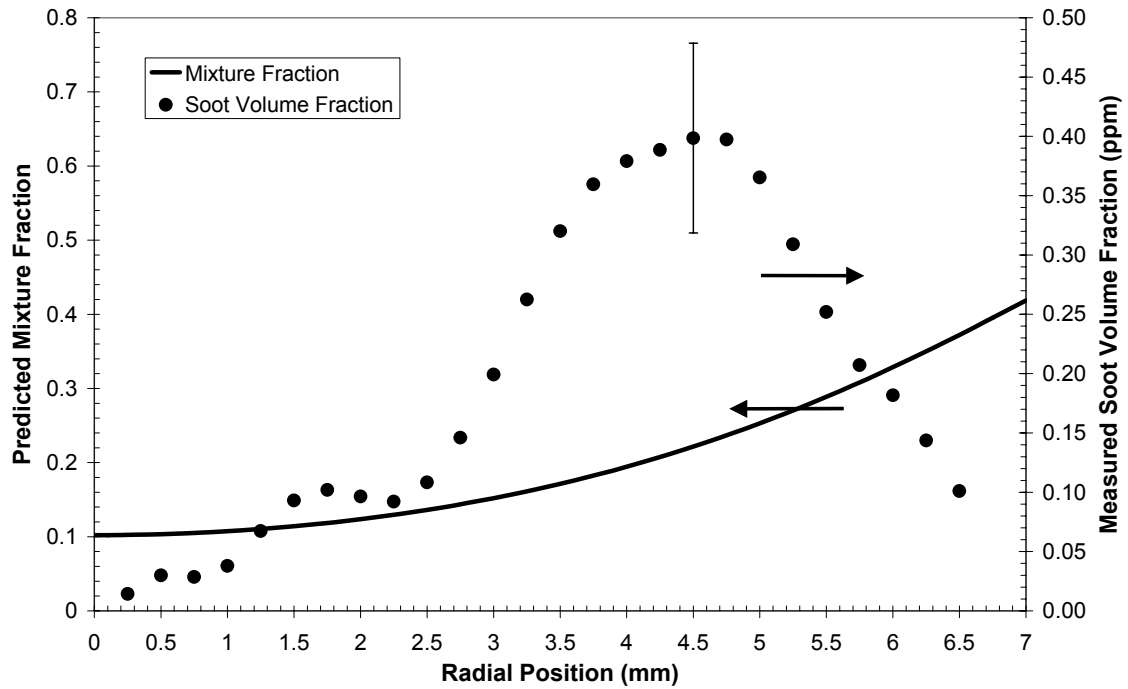

Figure 6. Measured Soot Volume Fraction and Predicted Mixture Fraction at 25-mm Axial Position, Ethylene IDF, 2.2-slpm Air
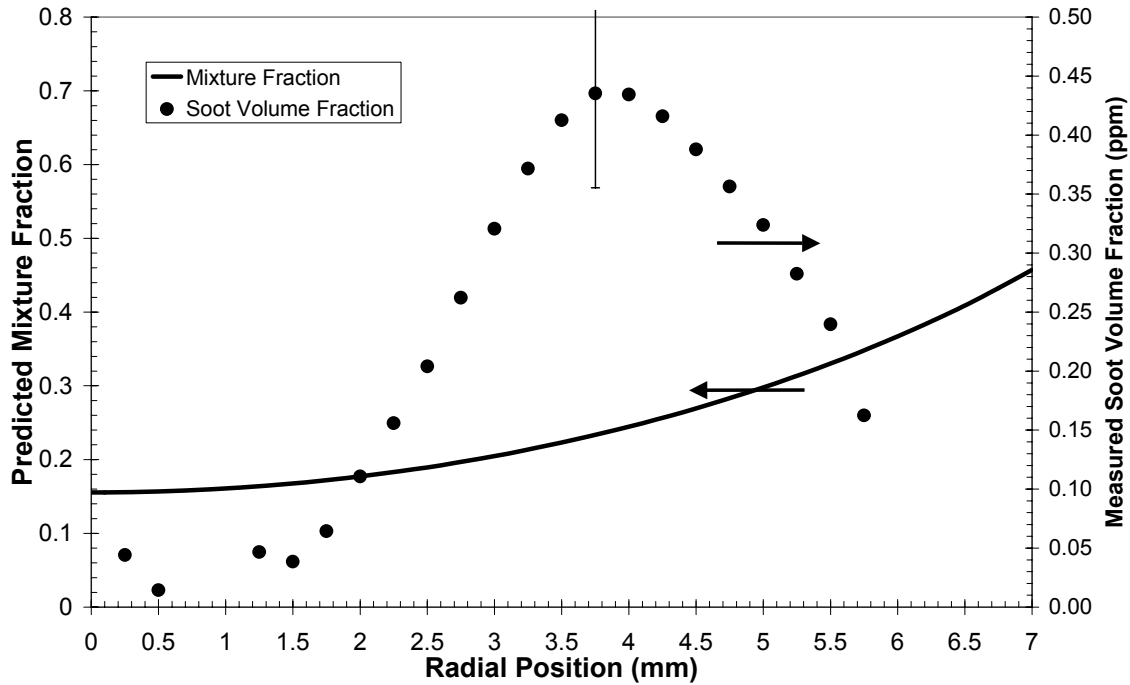
Figure 7. Measured Soot Volume Fraction and Predicted Mixture Fraction at 30-mm Axial Position, Ethylene IDF, 2.2-slpm Air

Figures 8-11 show radial profiles of measured soot volume fraction along with simulated flame temperatures for axial distances of 15 mm, 20 mm, 25 mm, and 30 mm. Vertical dotted lines marking the locations of the stoichiometric contour and the 1300 K minimum soot formation temperature are shown in the figures. For heights of 15 mm and 20 mm (below the flame tip), the temperature increases with radial distance, reaches a peak, and then decreases. For heights of 25 mm and 30 mm (downstream of the flame tip), temperature decreases gradually with radius. The peak in soot volume fraction corresponds to a simulated temperature of 1700, 1740, 1860, and 1800 K, respectively, for heights of 15, 20, 25, and 30 mm. At the lower heights of 15 and 20 mm (Figs. 8-9), soot is present primarily in regions where the predicted temperature is greater than the soot formation minimum temperature limit of 1300 K as suggested in the literature [17-19]. In summary, the soot concentration peaks are located where the local simulated temperature ranges from 1700 to 1860 K.
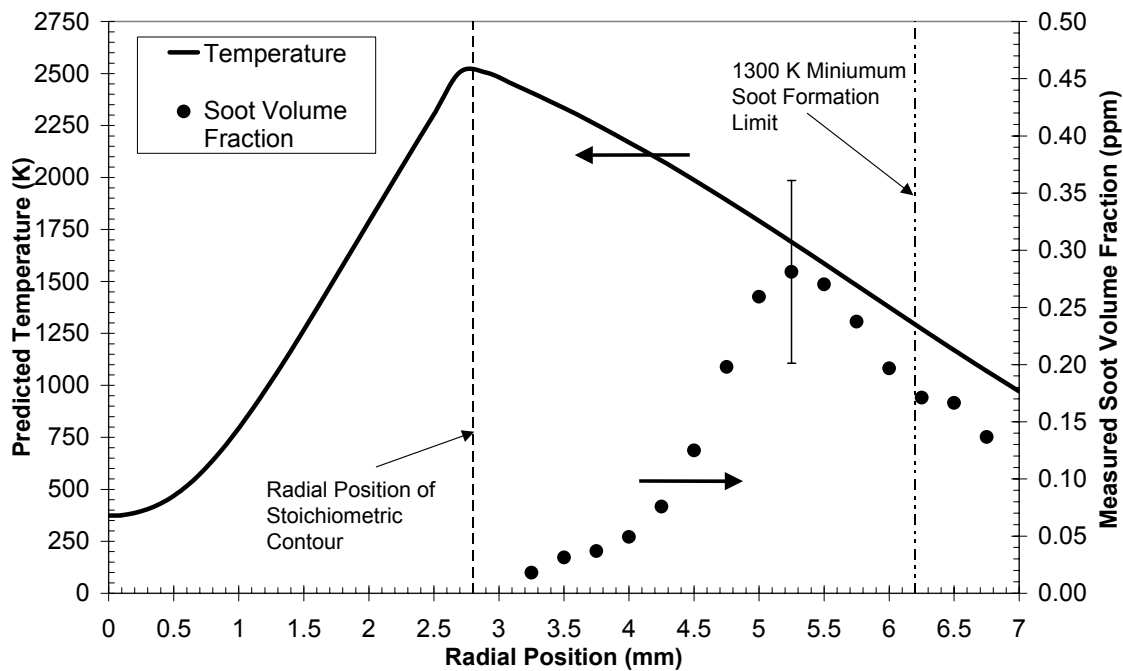
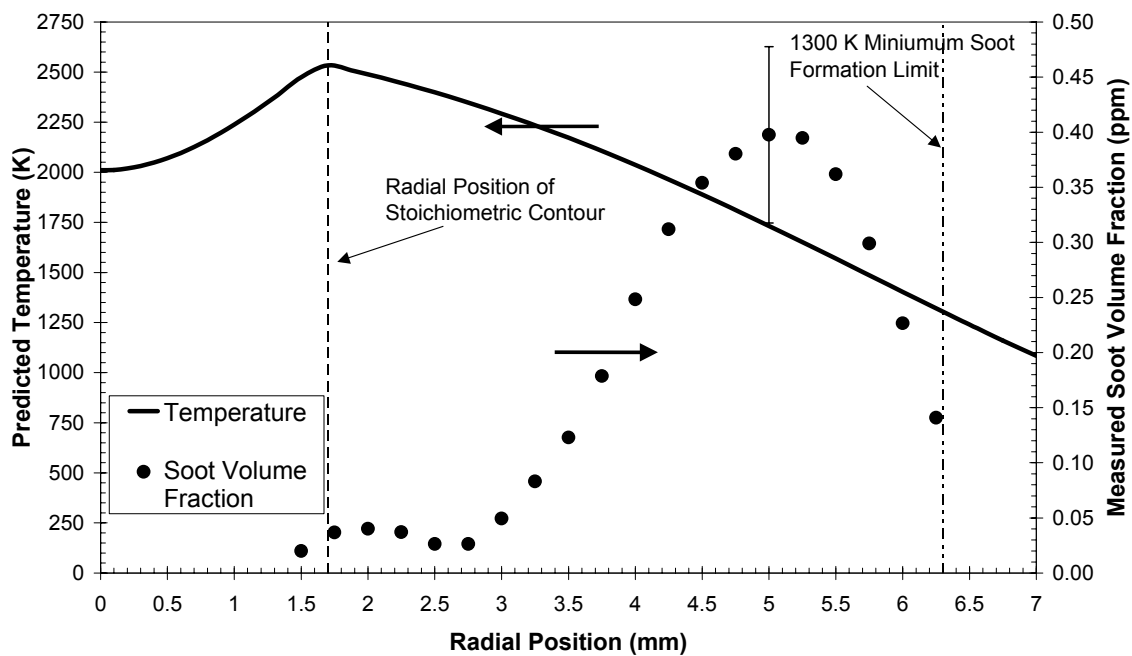**Figure 8. Measured Soot Volume Fraction and Predicted Temperature at 15-mm Axial Position, Ethylene IDF, 2.2-slpm Air**

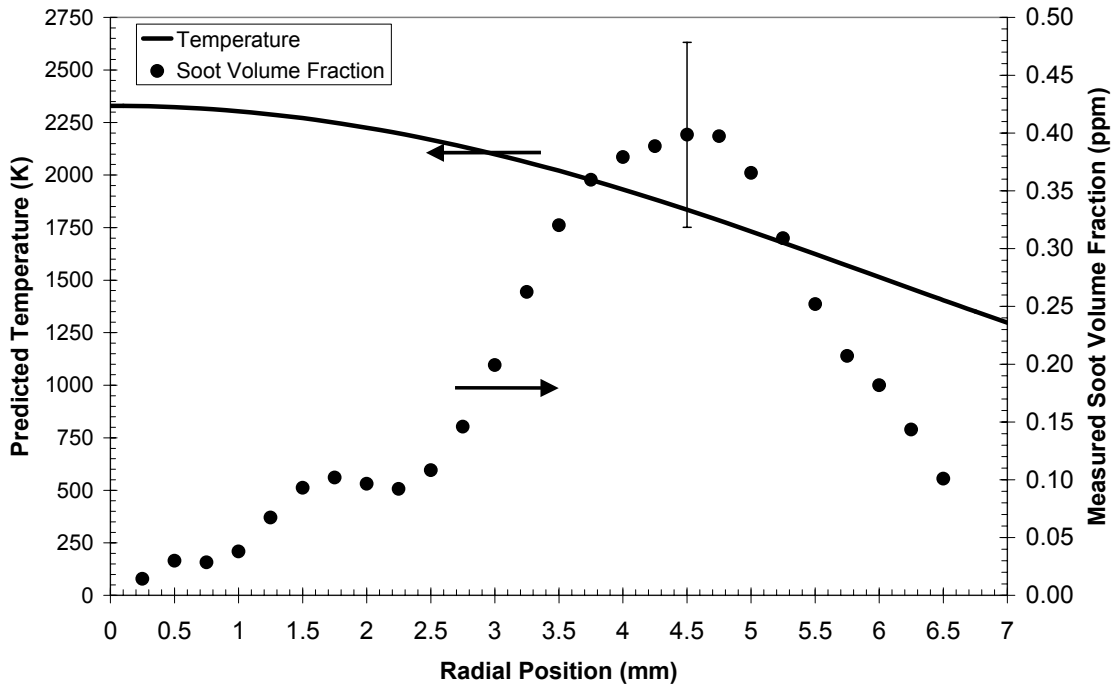**Figure 9. Measured Soot Volume Fraction and Predicted Temperature at 20-mm Axial Position, Ethylene IDF, 2.2-slpm Air**

Figure 10. Measured Soot Volume Fraction and Predicted Temperature at 25-mm Axial Position, Ethylene IDF, 2.2-slpm Air
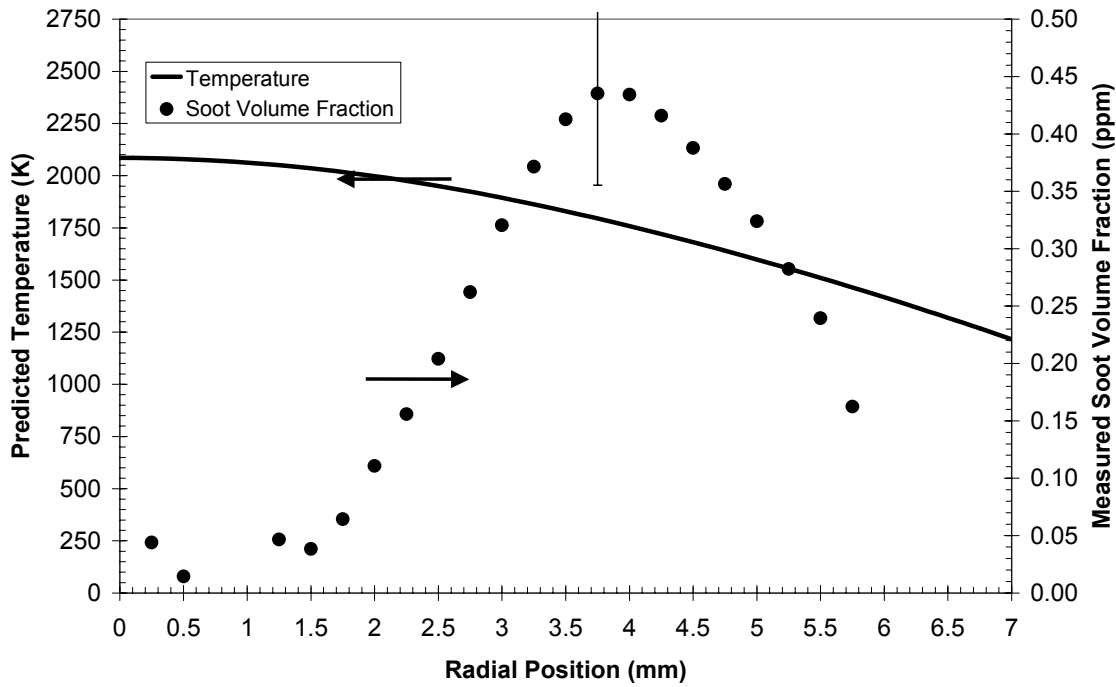

Figure 11. Measured Soot Volume Fraction and Predicted Temperature at 30-mm Axial Position, Ethylene IDF, 2.2-slpm Air

The radial soot volume fraction data were transformed into an integrated soot volume fraction for each individual axial height using the following equation:

$$F_v(z) \equiv 2\pi \int_0^R r\, f_v(z,r)\, dr \qquad \text{Eq. 3}$$

where R (mm) is the outer radius of measurable soot and r (mm) is the radius at the local soot volume fraction, $f_v(z,r)$. This integrated soot volume fraction, F_v (mm^2), is a measure of the total amount of soot present in the flame at each height [7]. Figure 12 shows the integrated soot volume fractions with temperatures at soot concentration peaks at the tested heights. The unit for integrated soot volume fraction has been converted to (cm^2) for ease of comparison to previous studies. Data points are connected with lines to guide the eye in interpreting the graph. Low in the flame, integrated soot volume fraction increases with axial distance, peaking at a value of 3.2×10^{-7} cm^2 at a height of 25 mm and decreasing or remaining constant downstream of the peak. The results from this plot, combined with soot concentrations plotted radially in Figs. 4-11, are consistent with the previous result that soot forms on the fuel side of the flame, and after passing downstream of the flame, the soot concentration eventually levels off to some constant value. The rate of change in integrated soot volume fraction appears to be relatively constant with height until it reaches a maximum temperature near the height of the flame tip. The post-flame IDF results are in contrast to past NDF results, where the soot volume fraction tends to decrease sharply after the soot passes through the high temperature oxidation layer [7]. The IDF integrated soot volume fraction approaches a value of about 3×10^{-7} cm^2, which is similar in magnitude to the value of 2.5×10^{-7} cm^2, measured in IDFs by Makel and Kennedy [6]. Santoro *et al.* measured peak integrated soot volume fractions an order of magnitude higher (10^{-6} cm^2) in NDFs [18], suggesting that IDFs form less soot than NDFs. However, Shaddix *et al.* measured similar soot volume fractions in both IDFs and NDFs with a Wolfhard-Parker slot burner [2]. This difference in results could possibly be attributed to the different burner geometries, but further study is warranted.
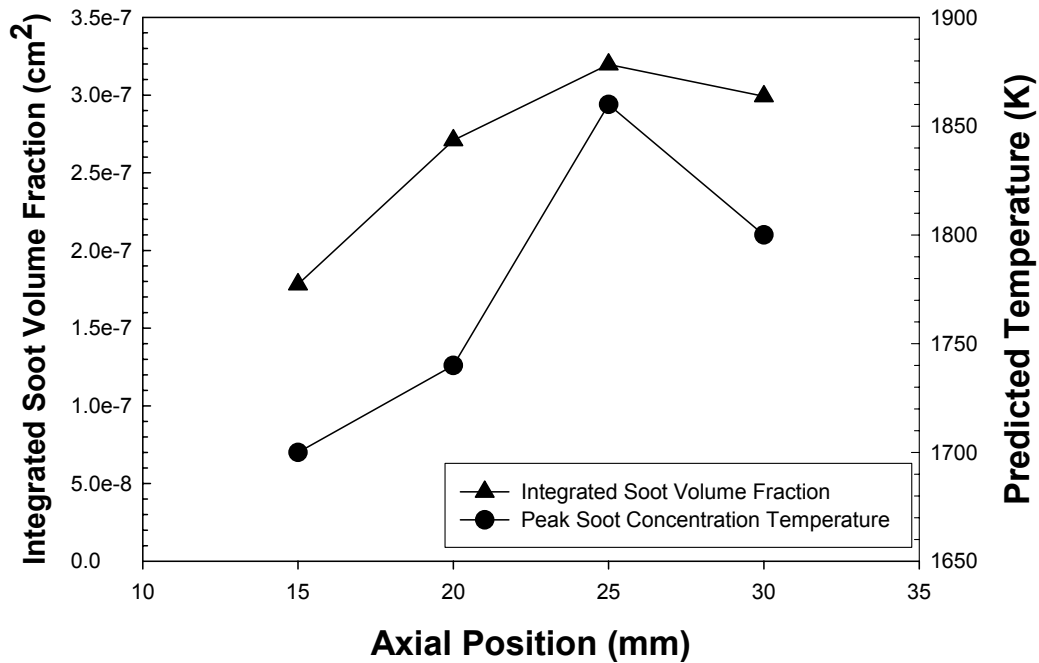
Figure 12. Radially Integrated IDF Soot Volume Fraction and Peak Soot Concentration Temperature

To better understand why the measured soot volume fraction in the IDF is an order of magnitude lower than the literature values for coflow NDFs, the tracer particles were employed in simulations of the IDF and an NDF. The simulated NDF flow rates (2.7 slpm air and 0.05 slpm fuel, leading to cold-flow velocities of 7.2 cm/s for air and 1.1 cm/s for fuel) were chosen to produce an average flame height similar to that of the IDF (~22 mm) and a similar air-to-fuel velocity ratio of 6.5. Additionally, the Froude number was kept low to provide a buoyancy-dominated flame similar to the IDF examined in this study. The IDF and NDF had Froude numbers of 0.42 and 1.2×10^{-6}, respectively. Fig. 13 shows a comparison of the IDF and NDF temperature maps. The NDF flame height is slightly greater than that of the IDF. The tracer particle trajectories are represented in the plots by black and white dots, which are spaced by 2 millisecond time intervals. It should be noted that these temperature maps are used only as qualitative tools to help explain reasons for soot formation.
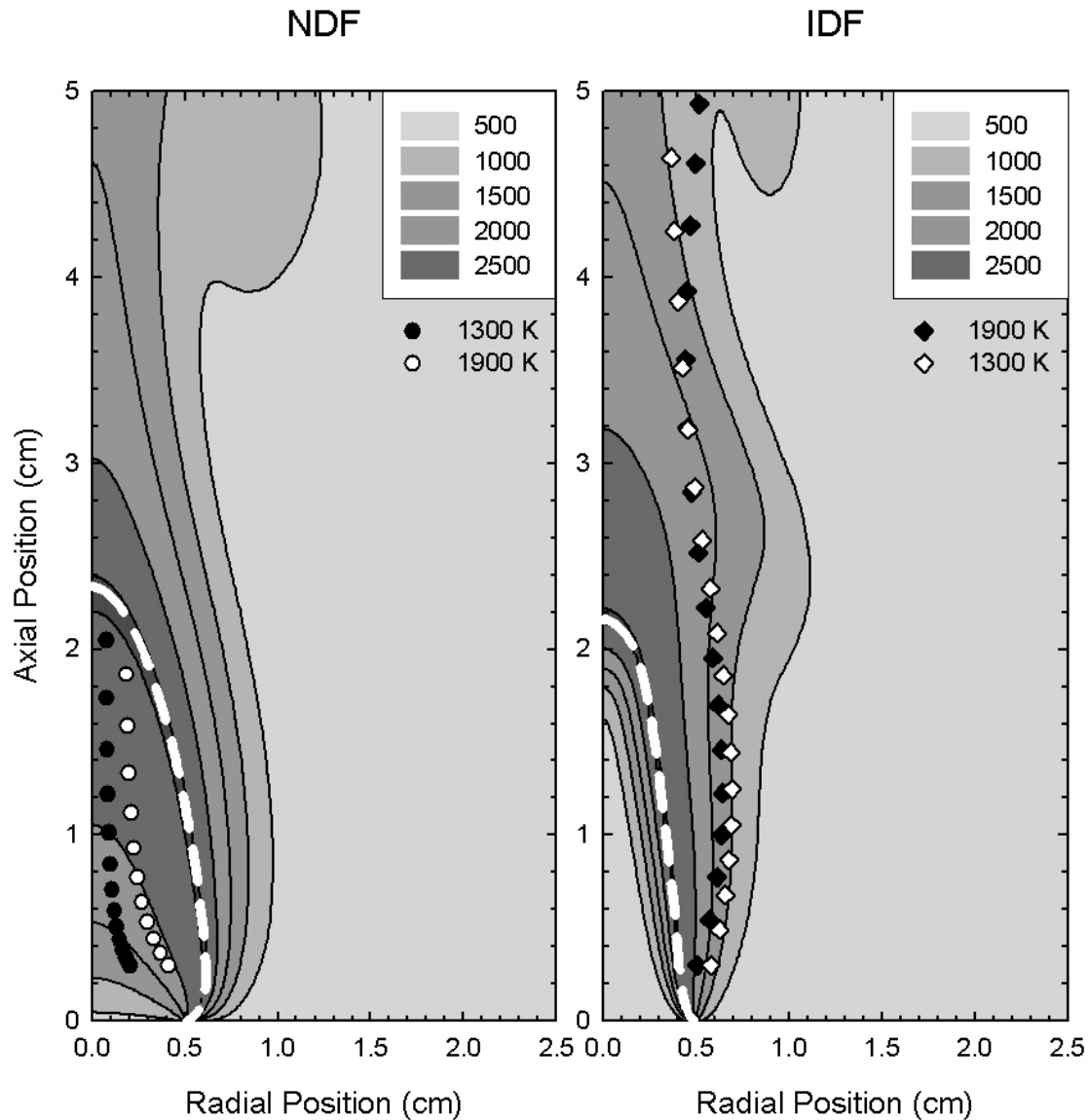
Figure 13. Predicted IDF (Ethylene 7.0 cm/s, Air 46.7 cm/s) and NDF (Ethylene 1.1 cm/s, Air 0.22 cm/s) Temperature Maps with Tracer Particle Trajectories Starting in Locations at 1300 K and 1900 K and 3 mm Axial Position

In the IDF, the tracer particles start near the flame and move farther away from the relatively thin high temperature reaction zone due to thermophoresis as their height increases. However in the NDF, the tracer particles are pushed inward by thermophoresis and stay in the relatively thick high temperature area for much longer as they move upward. This longer residence time in the high temperature zone for NDF soot particles may provide one explanation for the relatively higher measured peak soot concentrations in NDFs. The fuel in NDFs has more time for pyrolysis and soot growth at the high temperatures. However, many other factors go into the soot formation process, so this should not be considered a complete explanation for the differences in IDF and NDF soot concentrations.
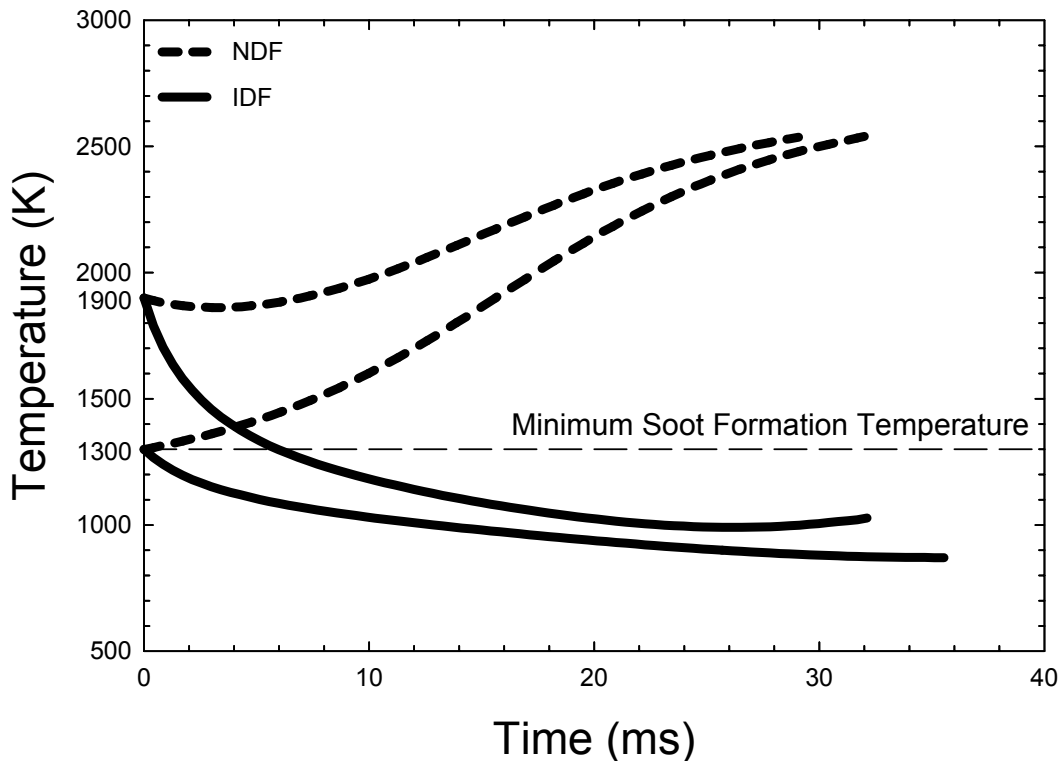
Figure 14. Time-Temperature Histories of Tracer Particles in Simulated NDF and IDF

Fig. 14 displays the temperatures encountered by the tracer particles as a function of time as they move upward in the simulated flames. The figure demonstrates that soot formed in the IDF immediately cools after it forms. If the soot forms at an inception temperature of 1300 K, its temperature stays below the minimum soot formation temperature over its lifetime. If it forms at 1900 K, it stays warmer than the minimum soot formation temperature for about six milliseconds. In contrast, the figure shows that soot formed in the NDF heats up after it forms, spending about 30 milliseconds above the minimum soot formation temperature, regardless of its inception temperature. The higher temperatures experienced over the lifetime of the soot in the NDF could lead to increased in-flame soot mass through enhanced particle inception and growth.

Conclusions
A He-Ne laser beam was projected through a cylindrical co-flowing ethylene IDF, and the extinction measurements were used to find radially resolved soot volume fractions. Peak soot volume fractions were measured to be on the order of one part per million, which is consistent in magnitude with those available in the literature for IDFs [2,6] and lower in magnitude than the peak values reported for coflow NDFs [7,8]. The soot volume fraction peaks occur between simulated mixture fractions of 0.22 and 0.26 and

16

between simulated temperatures of 1700 K and 1860 K. The soot volume fraction results confirm that soot formation occurs until some point slightly after the flame tip height, with soot concentration either decreasing slightly or leveling off to some nearly constant value as the soot particles quench without being oxidized. Simulation results show high temperature residence times to be greater in NDFs, which points to one explanation for the higher soot concentrations in NDFs relative to IDFs.

References

[1]. L.G. Blevins, R.A. Fletcher, B.A. Benner, E.B. Steel, G.W. Mulholland, Proceedings of the Combustion Institute 29 (2003) 2325-2333.

[2]. C.R. Shaddix, T.C. Williams, L.G. Blevins, R.W. Schefer, Proceedings of the Combustion Institute 30 (1) (2005) 1501-1508.

[3]. J.S. Lighty, J.M. Veranth, A.F. Sarofim, Journal of the Air & Waste Management Association 50 (9) (2000) 1565-1618.

[4]. B.S. Haynes, H.Gg. Wagner, Progress in Energy and Combustion Science 7 (4) (1981) 229-273.

[5]. P.S. Greenberg, J.C. Ku, Applied Optics 36 (22) (1997) 5514-5522.

[6]. D.B. Makel, I.M. Kennedy, Combustion Science and Technology 97 (4-6) (1994) 303-314.

[7]. R.J. Santoro, H.G. Semerjian, R.A. Dobbins, Combustion and Flame 51 (2) (1983) 203-218.

[8]. C.R. Shaddix, K.C. Smyth, Combustion and Flame 107 (4) (1996) 418-452.

[9]. J.H. Kent, H.G. Wagner, Combustion and Flame 47 (1) (1982) 53-65.

[10]. C.R. Shaddix, J.E. Harrington, K.C. Smyth, Combustion and Flame 99 (3-4) (1994) 723-732.

[11]. M.A. Mikofski, T.C. Williams, C.R. Shaddix, L.G. Blevins, Western States Section 2004 Spring Meeting, The Combust. Inst. Paper 04S-7r. http://repositories.cdlib.org/cpl/mc/MikofskiWSS04/.

[12]. C.J. Dasch, Applied Optics 31 (8) (1992) 1146-1152.

[13]. R.J. Santoro, Shaddix C.R., in: K. Kohse-Höinghaus, J.B. Jeffries (Eds.), Applied Combustion Diagnostics, Chapter 9: Laser-Induced Incandescence, Taylor & Frances, New York, 2002, p. 252.

[14]. K.C. Smyth , C.R. Shaddix, Combustion and Flame 107 (3) (1996) 314-320.

[15]. C.L. Tien, S.C. Lee, Progress in Energy and Combustion Science 8 (1) (1982) 41-59.

[16]. T.T. Charalampopoulos, H. Chang, Combustion Science and Technology 59 (4-6) (1988) 401-421.

[17]. J. Du, R.L. Axelbaum, Combustion and Flame 100 (3) (1995) 367-375.

[18]. R.J. Santoro, T.T. Yeh, J.J. Horvath, H.G. Semerjian, Combustion Science and Technology 53 (2-3) (1987) 89-115.

[19]. A. Gomez, M.G. Littman, I. Glassman, Combustion and Flame 70 (2) (1987) 225-241.

[20]. R.W. Davis , E.F. Moore, R.J. Santoro, J.R. Ness, Combustion Science and Technology 73 (4-6) (1990) 625-635.

[21]. M.A. Mikofski, L.G. Blevins, R.W. Davis, E.F. Moore, G.W. Mulholland, in: Seventh International Workshop on Microgravity Combustion and Chemically Reacting Systems, NASA, 2003, p. 53.

[22]. R.W. Davis , E.F. Moore, M.R. Zachariah, Journal of Crystal Growth 132 (3-4) (1993) 513-522.

[23]. F.P. Incropera, D.P. Dewitt, Fundamentals of Heat and Mass Transfer, John Wiley & Sons, New York, NY, 1990.